2008

Estimation of Shelf-Slope Exchanges Induced by Frontal Instability Near Submarine Canyons

A. Jordi

John M. Klinck
Old Dominion University, jklinck@odu.edu

G. Basterretxea

A. Orfila

Estimation of shelf-slope exchanges induced by frontal instability near submarine canyons

A. Jordi,[1] J. M. Klinck,[2] G. Basterretxea,[3] A. Orfila,[3] and J. Tintoré[3]

Received 9 March 2007; revised 29 August 2007; accepted 3 January 2008; published 13 May 2008.

[1] The dynamics associated with the propagation of unstable waves along a density front and their interaction with submarine canyons are simulated and analyzed with a fine-resolution three-dimensional primitive equation coastal ocean model. Simulations consider flow in an alongshore density front over two bottom topographies: an idealized straight shelf and a shelf incised by a canyon. The stationary circulation over the idealized shelf exhibits a geostrophic balance that is perturbed when the canyon topography is introduced. Enhanced cross-shore and vertical motions are produced as a result of the front-canyon interaction. A second set of simulations consider the effect of a small perturbation superimposed on the frontal circulation which develops growing meanders. In this case, the perturbation over the shelf grows rapidly by baroclinic instability into a steepened backward breaking wave characterized by significant cross-shore and vertical motions. The canyon topography accelerates or slows the development of the perturbation depending on the relative position of the unstable waves and the canyon. Finally, we use model results to determine the shelf-slope exchanges based on two methodologies. The first method computes the water transported across the shelf break while the second accounts for cross-shore displacements of water. The application of both approaches reveals that not all water transported across the shelf break is effectively exchanged between the shelf and the open ocean. However, cross-shore and vertical motions are enhanced by the unstable front and the submarine canyon leading to a large exchange between shelf and open ocean waters.

Citation: Jordi, A., J. M. Klinck, G. Basterretxea, A. Orfila, and J. Tintoré (2008), Estimation of shelf-slope exchanges induced by frontal instability near submarine canyons, *J. Geophys. Res.*, *113*, C05016, doi:10.1029/2007JC004207.

1. Introduction

[2] The exchange of water, solutes and particles between the coastal area and the open sea is of topical interest for global biogeochemical fluxes, budgets and their response to climate change and human activities [*Huthnance*, 1995]. Most continental shelf areas are relatively isolated from the open ocean by energetic slope currents, which are in quasi-geostrophic balance and follow isobaths; thus, acting as barriers to shelf-slope exchange. However, frontal instabilities together with abrupt changes in bathymetry can induce important ageostrophic motions, leading to significant exchange of water and its constituents across the shelf break.

[3] Slope fronts are well recognized features of the circulation over the continental shelf. They arise from a variety of physical mechanisms, such as density differences between lower-salinity shelf waters that result from continental runoff, and denser open-seawaters. The location of fronts is usually modified by the meanders of either dynamic or topographic origin that can grow and develop into eddies. Previous studies have recognized meandering and instability of frontal jets as important processes in creating frontal variability, mesoscale upwelling and cross-frontal exchange [*Spall and Richards*, 2000; *Gawarkiewicz et al.*, 2004]. The formation and evolution of these meanders on fronts is caused by a combination of barotropic and baroclinic instability [*Onken*, 1992].

[4] Observations and numerical models provide evidence of large vertical velocities associated with frontal meandering and instabilities. *Wang* [1993] describes upwelling motions occurring in the meander crests and subduction in the meander troughs. Frontal variability also produces different regimes of shelf-slope exchange over relatively small space and timescales [*Álvarez et al.*, 1996; *Gawarkiewicz et al.*, 2004]. Estimates of shelf-slope fluxes indicate larger cross-shore transports than previously thought. For example, *Huthnance* [1995] estimated that the whole volume of shelf water in the northwest Iberian margin is exchanged in approximately 12 days mostly due to frontal meanders and filaments.

[5] In addition to slope fronts, shelf topography is a key element controlling the circulation over the continental

[1]Marine Sciences Research Center, State University of New York, Stony Brook, New York, USA.
[2]Center for Coastal Physical Oceanography, Old Dominion University, Norfolk, Virginia, USA.
[3]IMEDEA (CSIC-UIB), Institut Mediterrani d'Estudis Avançats, Esporles, Illes Balears, Spain.

0148-0227/08/2007JC004207

margin and the shelf-slope exchange. Significant topographic features accelerate the development of meanders and instabilities on fronts and introduce a diversity in scales [*Tintoré et al.*, 1990; *Péliz et al.*, 2003]. Topography controls the cross-shelf flows since there is a significant correlation between the curvature of the shelf break and the transport across the shelf break [*Dinniman et al.*, 2003]. In this context, submarine canyons are one of the most prominent topographic features that are known to modify physical and, consequently, chemical, biological and geological processes in their vicinity [*Inman et al.*, 1976].

[6] The spatial pattern of regional upwelling and the shelf-slope exchange of water and material are enhanced by submarine canyons [*Hickey*, 1997]. The circulation within and near canyons is further complicated by interaction of coastal fronts and canyon topography. Cyclonic vorticity, associated with shelf water sinking into the canyon, occurs near the shelf edge in the upstream side whereas anticyclonic vorticity occurs in the downstream side [*Hickey*, 1995]. The magnitude of vertical and cross-slope motions is, to a large extent, determined by water column stratification [*Klinck*, 1996]. The wind and frontal variability are also responsible for a remarkable modification of the circulation in the vicinity of the canyon and produce increases of cross-shore transports and vertical motions [*Ardhuin et al.*, 1999; *She and Klinck*, 2000].

[7] Modeling studies of submarine canyons usually address the interaction of density or wind-driven flows with the canyon topography; however, the problem of the interaction of frontal instability with submarine canyons has been rarely addressed. *Jordi et al.* [2005a] analyze a meander associated with an stable front and its interaction with the Palamós submarine canyon using a three-dimensional primitive equation coastal ocean model. They find that shelf-slope exchanges are enhanced as a result of the interaction of the meander with the canyon.

[8] The purpose of this study is to extend the results of *Jordi et al.* [2005a] to unstable fronts and examine the effects of canyon topography on the development of instabilities. Here, we use an idealized topography in order to isolate the influence of unstable fronts and submarine canyons on the shelf circulation. We analyze the circulation pattern generated by an unstable front over an idealized shelf and the modifications produced by the interaction of the frontal jet and its meanders with a submarine canyon. Our final objective is to estimate the magnitude of shelf-slope exchange generated by the interaction between the unstable frontal flow and the submarine canyon.

[9] We have also limited the study to the conditions of the northwestern Mediterranean shelf, where the continental margin is repeatedly bisected by submarine canyons that cut across about 60% of the continental margin. The regional oceanography is dominated by a permanent density front located on the continental margin which forms the northern branch of circulation in the northwestern Mediterranean, called Northern Current [*Millot*, 1999]. Satellite images and data collected in the area reveal that the cyclonically flowing Northern Current is characterized by strong mesoscale variability, forming meanders and shedding eddy-like structures, thought to be due to baroclinic instability [*La Violette et al.*, 1990; *Rubio et al.*, 2005].

2. Methods

2.1. Model Description

[10] The numerical model used in this study is based on a three-dimensional primitive equation coastal ocean general circulation model of *Wang* [1982] and *Wang* [1997]. It is formulated in a constant z coordinate. Model variables are the three components of the flow, density and surface height. The temperature array in the model is used for pseudo-density and the specification of a linear equation of state with a thermal expansion coefficient of unity makes the temperature and density equivalent. The model uses a centered difference scheme in the momentum equations and flux-corrected transport for the temperature. The model has been used in several studies including circulation over coastal submarine canyons [*Ardhuin et al.*, 1999; *Jordi et al.*, 2005a] and dynamics of frontal jet instability [*Wang*, 1993].

[11] The model domain is 100 km across-shore (x direction) and 300 km alongshore (y direction). The model uses constant horizontal resolution of 1 km and vertical resolution of 25 m. The Coriolis parameter is assumed constant ($f = 9.7 \times 10^{-5}$ s^{-1}). The time integration is based on a split-mode calculation with time intervals of 1 s for the external mode and 30 s for the internal mode. The horizontal eddy coefficient is constant ($\nu = 10$ m^2/s) and the vertical eddy coefficients are computed from an embedded mixed layer model using Mellor-Yamada level 2 turbulence closure [*Chen et al.*, 1988], which allows vertical viscosity and diffusivity to be as small as 0.1 cm^2/s.

[12] The coast is placed at the left boundary ($x = 0$). The domain is periodic in the alongshore direction representing continuation between the upstream boundary ($y = 100$ km) and the downstream boundary ($y = -200$ km). At the offshore open boundary ($x = 100$ km), the normal gradient of velocity and the surface elevation are each set to zero. There is no surface forcing. At the solid boundaries, the normal velocity is set to zero (a slip boundary). A quadratic law is used for bottom friction with a drag coefficient of $C_d = 3 \times 10^{-3}$.

2.2. Model Bathymetry

[13] Two bathymetric configurations are used representing an idealized shelf uniform in the alongshore direction (shelf topography) and the same shelf bathymetry incised by a submarine canyon (canyon topography). The shelf topography (H_s) is constructed from a sloping continental shelf (a cubic polynomial) connecting to the slope (a hyperbolic tangent) (Figures 1a and 1b).

$$H_s = \begin{cases} H_1 - H_1\left(\dfrac{(x - x_1)}{x_1}\right)^3 & \text{for } x \le x_1 \\ H_1 + \dfrac{H_2 - H_1}{2}\left[1 + \tanh\left(\dfrac{x - x_2}{L_1}\right)\right] & \text{for } x > x_1 \end{cases} \quad (1)$$

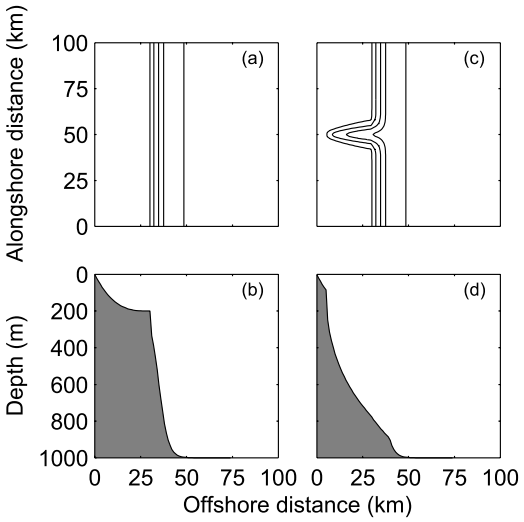

Figure 1. (a) Model domain and bathymetry for the shelf configuration. Only one third of the total (300 km) alongshore area is shown. The solid lines are isobaths with an interval of 200 m. (b) Bathymetric cross-section along the offshore direction. (c) Model domain and bathymetry for the canyon configuration. Only the area surrounding the canyon is shown. (d) Bathymetric cross-section along the canyon axis.

[14] The canyon topography (H_c) incises both the continental shelf and slope (Figures 1c and 1d).

$$H_c = H_s + \max\left(0, H_3\sqrt{\frac{x-x_3}{x_1-x_3}} - H_s\right)\exp\left[-\left(\frac{y-y_3}{L_2+\frac{\sqrt{x}}{L_3}}\right)^2\right] \tag{2}$$

Parameter values used in these expressions are given in Table 1.

2.3. Initialization

[15] Two initial configurations are used representing an idealized shelf-slope front uniform in the alongshore direction (unperturbed front) and the same front perturbed to permit the formation and growth of meanders (perturbed front). The initial density field (Figure 2) representing the unperturbed front is modeled by the following mathematical expression

$$\sigma(x,y,z,t=0) = \sigma_0 - \frac{\Delta\sigma_0}{2}\left[2 - \tanh\left(\frac{x-x_0}{L_0}\right)\right]\exp\left(-\frac{z}{H_0}\right) \tag{3}$$

Table 1. Parameters for the Model Bathymetry (Equations (1) and (2))

Parameter	Description	Value
x_1	offshore shelf position	30 km
x_2	offshore slope position	35 km
x_3	offshore canyon position	5 km
y_3	alongshore canyon position	50 km
L_1	slope width scale	5 km
L_2	canyon length scale	2 km
L_3	canyon width scale	12 km
H_1	shelf depth	200 m
H_2	open ocean depth	1000 m
H_3	canyon depth at the mouth	800 m

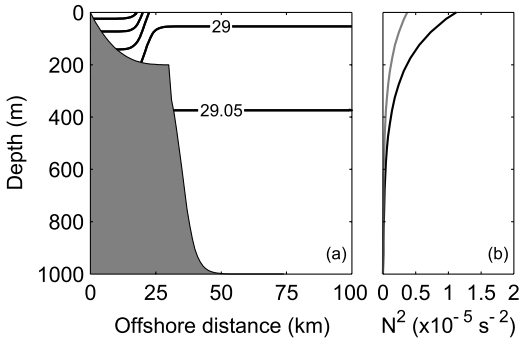

Figure 2. (a) Vertical section of the density (in σ_t units) at the initial time. The contour interval is 0.05 σ_t units. (b) Profiles of Brunt-Väisälä frequency squared near the coast (black line) and at open ocean (grey line).

where the homogeneous background density (σ_0) is 29.06, the across-front density contrast ($\Delta\sigma_0$) is 0.08, the offshore front position (x_0) is 20 km, the front width scale (L_0) is 3.2 km, and the scale for the front change with depth (H_0) is 180 m, which controls stratification. To generate the perturbed front, a small disturbance varying sinusoidally in the alongshore direction is added to the offshore front position

$$x_0 = 20\,km + A_d\cos\left(\frac{2\pi}{L_d}(y+\psi_d)\right) \tag{4}$$

where the amplitude of the disturbance (A_d) is 1 km (1 grid size), the wavelength of the disturbance (L_d) is 50 km, and the phase of the disturbance (ψ_d) is variable.

[16] Further, the geostrophic currents (relative to the bottom at 1000 m) associated with density fields (and ignoring the bottom topography) are computed before the first time step.

2.4. Errors

[17] Periodic boundary conditions are a source of error in the numerical model because disturbances created within the model cannot advect or radiate out of the model, but rather reappear upstream contaminating the results. These disturbances are due to gravity waves, coastal trapped waves and advection. Gravity waves are very fast but are generally small in amplitude. The first three modes of coastal trapped waves travel at velocities of 2.4, 0.9 and 0.4 m/s [*Jordi et al.*, 2005b] but the effects are also small in the first 20 model days. Advection does not represent a problem for the shelf topography because no disturbance is created. However, the initial adjustment between the front and the canyon topography creates a perturbation that propagates southward. The domain has been selected to be large enough (300 km) to prohibit any advected wrap-around affects due to periodic boundaries during the time of interest. Also, disturbances applied initially to generate the perturbed front will reappear upstream due to periodic conditions; but this effect is required to allow the propagation of frontal instabilities.

2.5. Cases

[18] Four cases are described in this paper, representing a unperturbed front over shelf topography (case 1), a unper-

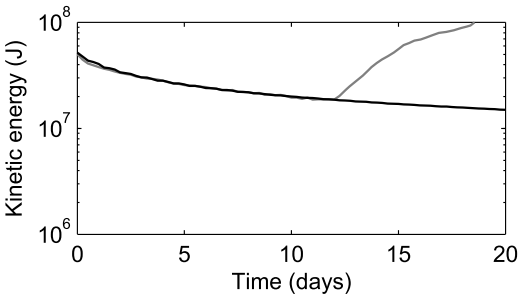

Figure 3. Time evolution of the mean kinetic energy (J) between alongshore locations 25 and 75 km for case 1 (black line) and case 2 (grey line).

turbed front over canyon topography (case 2), a perturbed front over shelf topography (case 3), and a perturbed front over canyon topography (case 4). There are two subcases to case 4 taking into account the relative position of the perturbation with the canyon by modifying the phase of the disturbance. Two values are considered, $\psi_d = 0$ km (see equation (4)) corresponds to an initial wave trough over the canyon axis (case 4a) and $\psi_d = 25$ km to an initial wave crest over the canyon axis (case 4b). The focus of the study is the shelf circulation in which we examine the effect of unperturbed/perturbed fronts and submarine canyon topography on this circulation.

2.6. Shelf-Slope Exchange

[19] In order to quantify the volume of water transported across the shelf break, the horizontal transport is calculated at each alongshore location across a vertical plane parallel to the coast located 30 km offshore and between alongshore locations 25 km to 75 km. Note that this plane coincides with the shelf break in the shelf topography, but it crosses the canyon mouth in the canyon topography. Horizontal transport is computed by integrating the cross-shore velocity across this plane with positive transport being offshore.

[20] However, this approach does not take into account the water displaced in one direction and subsequently transported in the opposite one. Therefore a critical issue is the magnitude of the net exchange. To address this question, we implement into the numerical model an Eulerian passive tracer that takes into account the cross-shore displacements of water. The tracer satisfies the advection diffusion equation, which is solved with the same numerical scheme used for temperature. In the course of the model calculation (at time t_1), the tracer value at each grid point is set to be equal to the offshore distance from that grid point to the shore. The difference between the tracer at time t_2 and t_1 represents the net cross-shore displacement of the water. Positive values for the tracer difference means offshore displacements of water.

3. Results

3.1. Case 1: Unperturbed Front Over Shelf Topography

[21] This simulation represents the simplest case where currents are in geostrophic balance with the initial shelf break front giving an alongshelf flow of 30 cm/s (not shown). Outside the density front, currents are negligible. Figure 3 shows the time evolution of mean kinetic energy which has an e-folding decay timescale of about 18.4 days due to mixing and bottom friction.

3.2. Case 2: Unperturbed Front Over Canyon Topography

[22] The circulation at the surface does not react strongly to the upstream wall of the canyon (Figure 4). However, the jet veers offshore over the downstream wall of the canyon and becomes wider. This deflection is more noticeable in the offshore side of the jet where stratification is weaker. Downstream of the canyon the jet adjusts back to the shelf topography and flows parallel to the isobaths. Vertical movements are also influenced by the canyon. The motion is downward on the upstream wall and upward on the downstream edge, reaching velocities of up to 5 m/day.

[23] The previous description assumes that the circulation is steady after about 5 days. The initial alongshore circulation at the surface becomes progressively deflected in the vicinity of the submarine canyon until it reaches steady state around day 4. After this time the circulation changes very slowly until day 12, when the disturbance created by the canyon in the initial adjustment reaches the downstream boundary and reenters into the domain due to periodic continuation in the alongshore direction. This disturbance grows with time until it completely masks the steady state as shown in the evolution of the mean kinetic energy in the vicinity of the canyon (Figure 3).

3.3. Case 3: Perturbed Front Over Shelf Topography

[24] The time evolution of horizontal velocity and density fields at the surface and the vertical velocities at 100 m depth are shown in Figure 5. Early in the model run, perturbations grow rapidly disturbing the initial (strictly

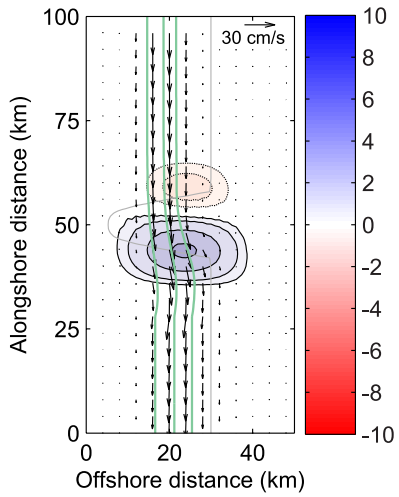

Figure 4. Horizontal velocity (vectors, in cm/s) at surface and vertical velocity (blue shaded with solid black line contours are upward velocity, and red shaded with dotted black line contours are downward, in m/day) at 100 m depth on model day 7.5 for case 2. Vectors are plotted at every fourth grid point. The 28.85, 28.90 and 28.95 (σ_t units) isopycnals (from coast to open ocean, respectively) at surface are represented with thick green lines. The 200 m isobath is plotted with a thin grey line.

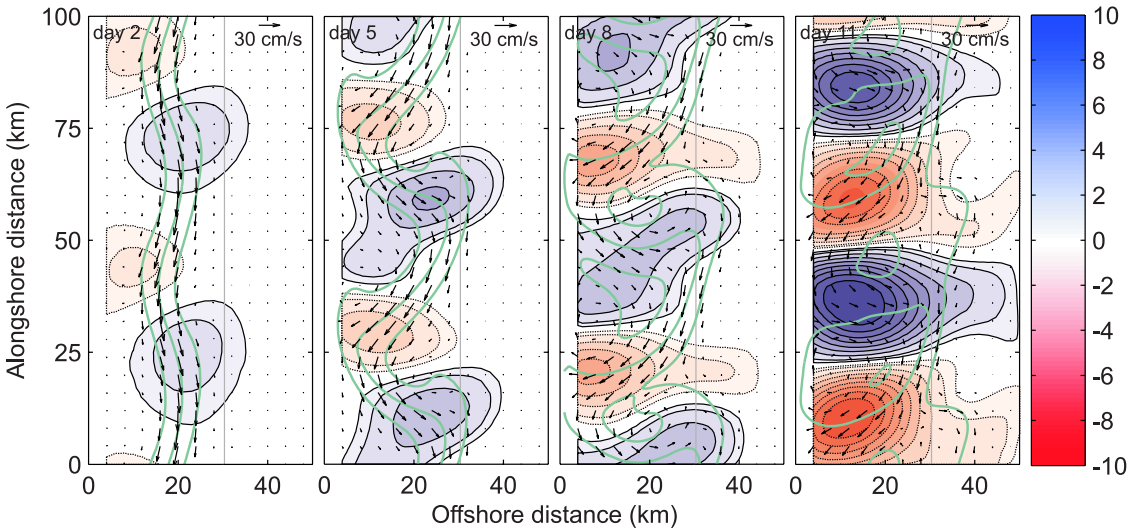

Figure 5. Horizontal velocity (vectors, cm/s) at surface and vertical velocity (blue shaded with solid black line contours are upward velocity, and red shaded with dotted black line contours are downward, in m/day) at 100 m depth on days 2, 5, 8 and 11 for case 3. Vectors are plotted at every fourth grid point. The 28.85, 28.90 and 28.95 (σ_t units) isopycnals (from coast to open ocean, respectively) at surface are represented with thick green lines. The 200 m isobath is plotted with a thin grey line.

alongshore) orientation of the front. Horizontal currents tend to follow the density field although there are departures from this pattern in the flow around wave troughs and crests. We define the wave troughs as the excursion of the jet toward the coast and the wave crest toward the open ocean. On day 5, these departures become so large that crests and troughs are bent backward enclosing isolated eddies that are clearly observable on day 8. Vertical movements are also modified by the development of unstable waves. Upwelling and downwelling areas are clearly separated with upward motion at wave crests and downward motion at wave troughs. In addition, vertical movements become more and more widespread and intense as the unstable waves grow, reaching speeds of 10 m/day on day 11. These strong currents are responsible for the mixing of the front on day 12.

[25] The development and decline of the unstable waves can be followed by the evolution of the perturbation amplitude (Figure 6). Amplitude is calculated as half of the cross-shore excursion of the surface 28.9 isopycnal (σ_t units) between the wave crest and the wave trough. Three phases can be distinguished: growth, equilibrium and relaxation. During the growing phase, instabilities develop until day 6 at a growth rate of 0.45 day^{-1}. During the equilibrium phase, the circulation is more or less steady between day 6 and 12 with southward propagating eddies having a constant amplitude, but it continues to change under the influence of mixing. Finally, the mixing is so strong on day 12 that it extinguishes the eddies.

3.4. Case 4: Perturbed Front Over Canyon Topography

[26] Figure 7 shows the evolution of horizontal velocity and density at the surface and vertical velocities at 100 m depth for the case 4a. The initial shape of the front over the canyon is defined by two opposite effects. The tendency of the wave trough to progress toward the coast is compensated by the offshore deflection induced by the canyon. As a result, the wave trough does not grow until it is out of the canyon influence and a wave crest approaches the canyon. Now, both the wave crest and the canyon tend to transport water offshore resulting in a faster growing wave crest.

[27] The evolution of the case 4b is different from the previous case (Figure 8). During the first few days, the additive effects of the unstable wave and the canyon topography accelerate the development of the wave crest toward the open ocean. However, from day 5 onward the effect of the wave trough and the canyon acts in opposite directions resulting in a more stable wave trough.

[28] In both cases (Figures 7 and 8), the vertical movements at 100 m depth present complicated patterns because the vertical speed generated by the frontal instability interacts with the vertical speed caused by the canyon topography. However, the canyon modifies the structure of vertical movements resulting in less intense and more widespread vertical motions on day 11 compared with the corresponding vertical motions for the case 3.

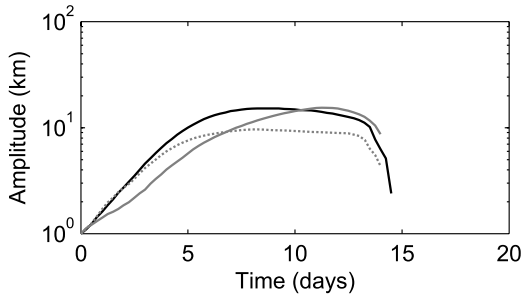

Figure 6. Time evolution of the amplitude (km) for case 3 (solid black line), case 4a (solid grey line) and case 4b (dotted grey line).

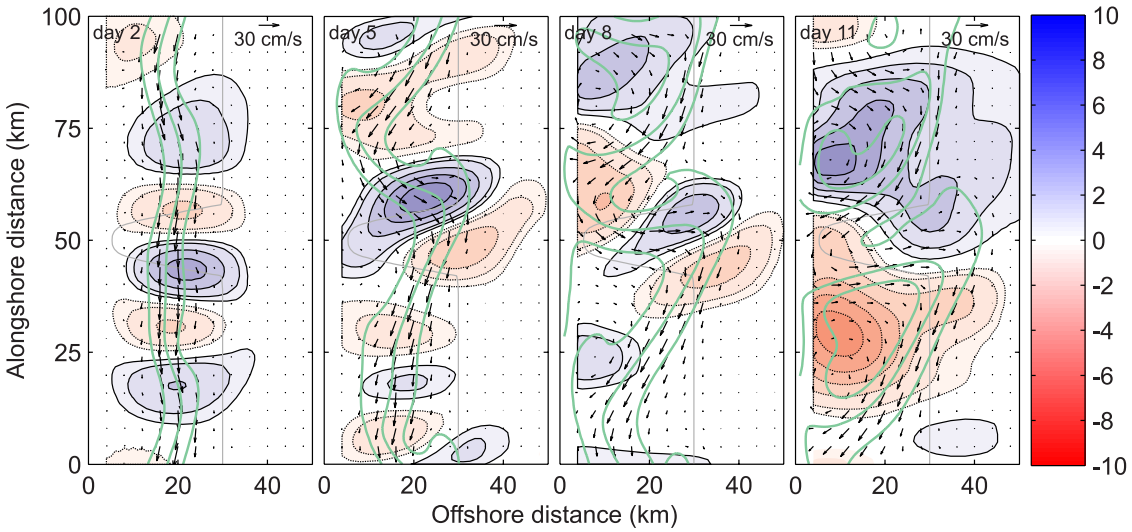

Figure 7. Horizontal velocity (vectors, cm/s) at surface and vertical velocity (blue shaded with solid black line contours are upward velocity, and red shaded with dotted black line contours are downward, in m/day) at 100 m depth on days 2, 5, 8 and 11 for case 4a. Vectors are plotted at every fourth grid point. The 28.85, 28.90 and 28.95 (σ_t units) isopycnals (from coast to open ocean, respectively) at surface are represented with thick green lines. The 200 m isobath is plotted with a thin grey line.

[29] Differences in the development of the unstable waves for both cases is tracked by the evolution of the amplitude of the waves (Figure 6). During the first few days the development of the perturbation is regulated by the relative position of the wave trough or crest to the canyon axis. The tendency is reversed when the following wave trough or crests crosses the canyon. There are differences in the equilibrium phase. The unstable wave with the initial crest over the canyon encloses an eddy and the equilibrium phase is similar to that for the unstable wave over shelf topography, although the resulting amplitude is smaller. In contrast, the unstable wave with the initial trough over the canyon does not enclose eddies and the equilibrium phase does not appear for this wave. The amplitude grows until the mixing disrupts the flow. Curiously, there is no evidence that the disturbance created by the canyon circles the domain on day 12 (as it happens in the case 2), suggesting that the disturbance is suppressed by the frontal instabilities.

3.5. Shelf-Slope Exchange

[30] Figure 9 shows the volume of water transported across the shelf break (a vertical plane parallel to the coast located 30 km offshore and between alongshore locations 25 km to 75 km) between day 6 and 12. The across-shelf-

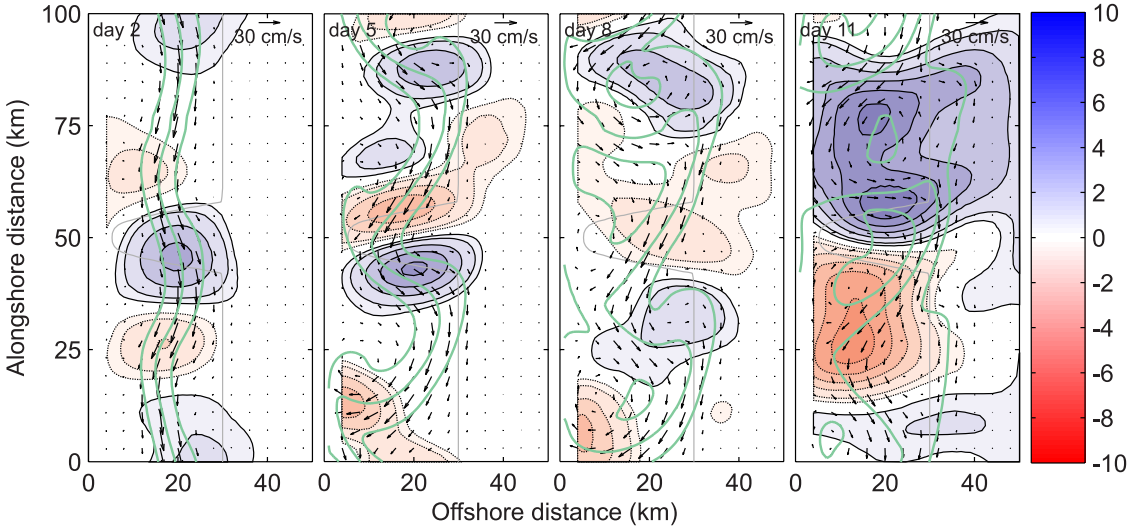

Figure 8. Horizontal velocity (vectors, cm/s) at surface and vertical velocity (blue shaded with solid black line contours are upward velocity, and red shaded with dotted black line contours are downward, in m/day) at 100 m depth on days 2, 5, 8 and 11 for case 4b. Vectors are plotted at every fourth grid point. The 28.85, 28.90 and 28.95 (σ_t units) isopycnals (from coast to open ocean, respectively) at surface are represented with thick green lines. The 200 m isobath is plotted with a thin grey line.

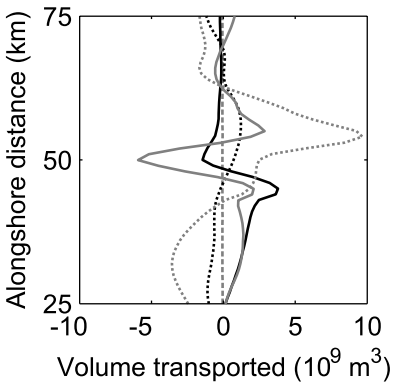

Figure 9. Volume of water transported between day 6 and 12 across a vertical plane parallel to the coast located at 30 km offshore and between alongshore locations 25 and 75 km for case 1 (dashed grey line), case 2 (solid black line), case 3 (dotted black line), case 4a (dotted grey line) and case 4b (solid grey line).

break transport for case 1 is small. The submarine canyon (case 2) creates onshore flow on the upstream side of the canyon and offshore flow downstream caused by the flow adjustments to the canyon (recall that the canyon axis is located at 50 km alongshore location). The onshore transport corresponds to an onshore flow at the deeper shelf levels on the upstream wall. Nevertheless, offshore flow is almost always larger than onshore resulting in a net offshore transport. Case 3 creates alternatively onshore and offshore flow associated with the development of meanders on both sides of the front, although the formation of isolated eddies disturbs somehow this general pattern. Finally, transports for case 4 depend totally on the relative position of the wave crests and trough with respect to the canyon. When a wave trough is initially over the canyon (case 4a), the water is transported offshore over the canyon and onshore downstream of it. In contrast, transport for case 4b is offshore upstream of the canyon and onshore over it.

[31] It is important to notice the onshore-offshore alternation of the flow along the shelf which suggests that water displaced in one direction would subsequently be transported in the opposite one. To address this question, we compute the cross-shore water displacements between days 6 (t_1) and 8 (t_2), as shown in Figure 10. The effect of case 2 on the cross-shore displacements is weak and associated with the offshore advection of the flow in the south wall of the canyon and the displacement downstream by the mean alongshore flow. Case 3 is responsible for onshore water displacements in the wave troughs and offshore displacements in the crests. In addition, there is an onshore transport where the wave crest bends backward. Finally, case 4a enhances the offshore displacement of water over the canyon and reduces it downstream the canyon. However, in case 4b the onshore water displacement downstream the canyon has reduced extension and magnitude. When t_2 is longer, the pattern of cross-shore displacements is also related to the development of unstable waves and to the canyon, but the magnitude of the displacement is greater.

[32] The tracer allows us to identify the volumes of water that experience a net displacement across the shelf break through the test vertical plane parallel to the coast 30 km offshore between alongshore locations 25 km to 75 km. This net displacement corresponds to water effectively exchanged and not only transported across the shelf break. Table 2 shows a comparison between the total volumes of water just transported and effectively exchanged (or displaced) between days 6 (t_1) and 12 (t_2) between the shelf and the open sea (offshore) and vice versa (onshore). The water transported by case 1 is negligible. Case 2 and case 3 create a similar offshore transport, but offshore and onshore transports caused by instabilities are balanced while the onshore transport caused by the canyon is about half of the offshore transport. Transports are slightly enhanced for cases 4a and 4b compared to the transports in case 3. With regard to the exchanged volumes of water, case 2 only exports water from the shelf to the open ocean. The exchanges produced by the unstable front are more significant, although the presence of the canyon affects slightly these exchanges enhancing offshore and decreasing onshore exchanges.

4. Discussion

4.1. Type of Instability

[33] The first question to be discussed is the type of instability that led to the observed meander growth on the

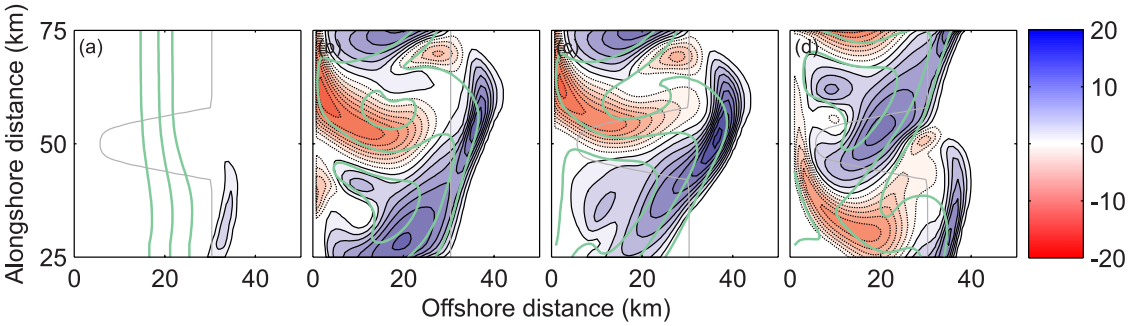

Figure 10. Cross-shore water displacement (blue shaded with solid black line contours are offshore displacements, and red shaded with dotted black line contours are onshore, in km) between days 6 and 8 at surface for (a) case 2, (b) case 3, (c) case 4a, and (d) case 4d. The 28.85, 28.90 and 28.95 (σ_t units) isopycnals (from coast to open ocean, respectively) at surface on day 8 are represented with thick green lines. The 200 m isobath is plotted with a thin grey line.

Table 2. Offshore and Onshore Volume of Water Transported and Exchanged Between Days 6 and 12 Across the Shelf Break (Units are 10^9 m^3) for Cases 1, 2, 3, 4a, and 4b

Volume		1	2	3	4a	4b
Transported	offshore	0.04	39.12	36.29	39.64	43.29
	onshore	0.00	20.60	37.93	45.13	38.78
Exchanged	offshore	0.00	13.75	23.30	25.00	24.05
	onshore	0.00	0.00	5.35	4.85	4.75

front. We analyze the energy budget using the formulation proposed by *Wang* [1993]. Solutions are separated into mean and perturbation, where the mean state is defined as an average over a wavelength and the perturbation is the difference between total and mean. The energy is integrated over the entire wavelength and over the entire water column. Figure 11 displays time series of energy conversions during the model run for case 3. The energy conversion from mean potential energy to eddy potential energy and from eddy potential energy to eddy kinetic energy are everywhere positive (with the exception of the first few days of simulation where the energy conversion from eddy potential energy to eddy kinetic energy is slightly negative). These positive values represent the energy flowing from the basic state to the perturbations via baroclinic instability. On the other hand, the energy conversion from mean kinetic energy to eddy kinetic energy is small, suggesting that the barotropic instability is small.

4.2. Comparison With Previous Theories and Studies

[34] To verify the model predictions and their consistency with previous instability theories, the stability of case 3 is examined using a two-dimensional inviscid linearized primitive equation model [*Xue and Mellor*, 1993]. Figures 12a and 12b show the growth rate and the phase speed for the most unstable mode displayed over a range of wavelengths. The corresponding results computed using the three-dimensional numerical model for different values of the wavelength of the disturbance (L_d, see equation (4)) show a good agreement with the linear predictions, although growth rate is overestimated for large wavelength and phase speed is also overestimated for small wavelength. It is interesting to note that while the growth rate curve contains the fastest-growing wave at a wavelength of 33 km, the maximum transport across the shelf break is obtained for a wavelength of 50 km (Figures 12a and 12c). For this reason, we use a disturbance with a wavelength of 50 km instead of 33 km for cases 3 and 4 because we are interested in shelf-slope exchanges.

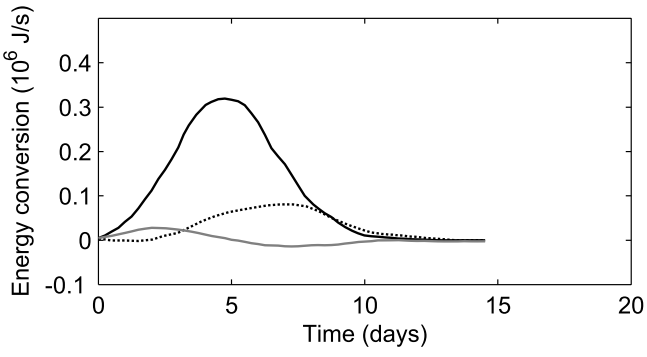

Figure 11. Time series of energy conversion from mean potential energy to eddy potential energy (solid black line), energy conversion from eddy potential energy to eddy kinetic energy (dotted black line) and energy conversion from mean kinetic energy to eddy kinetic energy (solid grey line) for case 3.

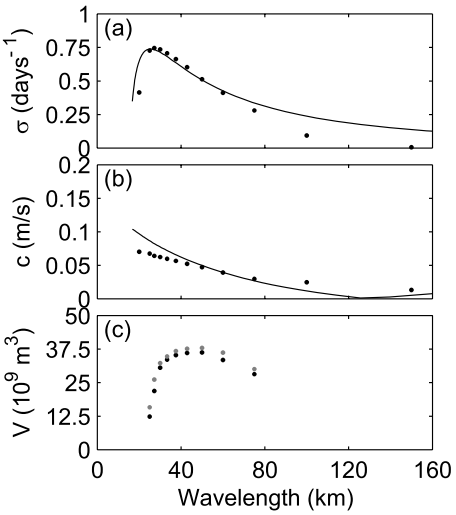

Figure 12. (a) Growth rate and (b) phase speed for the linear instability theory (black line) and for the model case 3 (black dots). (c) Volume of water transported offshore (black dots) and onshore (grey dots) across the shelf break for case 3.

[35] Several modeling and observational studies have investigated the effects of unstable fronts and submarine canyons on the shelf circulation. Our model for case 3 predicts upwelling on the wave crests and downwelling on the wave troughs, a typical feature of meandering flows, which has been investigated by *Onken* [1992], *Wang* [1993] and *Spall and Richards* [2000]. On the other hand, case 2 presents an anti-symmetrical structure of the flow with downwelling on the upstream side of the canyon followed by an upwelling on the downstream side, which was previously described by different authors [e.g., *Klinck*, 1996; *Skliris et al.*, 2002].

[36] *Jordi et al.* [2005a] studied the interaction of a stable frontal jet and its short-timescale variability with a canyon. They generated a propagating meander by displacing the slope front onshore. Since their front is stable, the meander should not grow. However, they observed that shelf-slope exchanges were enhanced in the vicinity of the canyon compared with the passing of the meander above a shelf that was not indented by a canyon. In view of our results, we interpret that their canyon forces the meander to grow (note that their case is similar to the case 4a). In contrast, when they remove the canyon from the topography, the meander does not develop and exchanges are reduced.

4.3. Shelf-Slope Exchange

[37] A primary motivation for this work is the estimation of the exchange of water across the shelf break associated with frontal instabilities and submarine canyons. One possible approach in this regard is to compute horizontal transports across a vertical plane formed by the shelf break and its projection on the surface [*Dinniman et al.*, 2003;

Table 3. Sensitivity Analysis for Cases 2, 3, and 4a Comparing the Volume of Water Transported Offshore (Tran, in 10^9 m^3), the Volume Exchange Offshore (Exch, in 10^9 m^3), Growth Rate (σ, in days^{-1}) and Phase Speed (c, in cm/s)[a]

	2		3				4a			
Parameter	Tran	Exch	σ	c	Tran	Exch	σ	c	Tran	Exch
base case	39.12	13.75	0.513	4.73	36.29	23.30	0.349	4.62	39.64	25.00
ν = 1 m^2/s	37.14	13.10	0.556	4.70	33.78	20.85	0.452	4.57	36.70	22.40
ν = 100 m^2/s	15.32	1.65	0.289	3.49	18.12	3.50	0.124	3.93	24.21	2.35
$C_d = 1 \times 10^{-3}$	47.26	16.55	0.531	5.05	40.95	24.65	0.404	4.99	39.99	25.60
$C_d = 5 \times 10^{-3}$	34.01	11.85	0.498	4.46	34.37	22.70	0.372	4.02	31.32	19.20
H_0 = 90 m	11.04	5.65	0.220	1.93	8.04	3.60	0.150	1.69	12.50	3.40
H_0 = 360 m	79.53	16.15	1.222	9.15	90.97	44.80	0.789	7.61	99.39	52.15
L_0 = 1.6 km	29.22	7.45	0.690	6.44	46.55	29.75	0.589	5.75	49.01	31.50
L_0 = 6.4 km	43.50	18.65	0.299	4.22	14.34	7.45	0.200	3.96	22.25	8.85
H_1 = 100 m	45.56	22.25	0.581	4.15	27.44	16.95	0.674	4.20	27.35	20.60
H_1 = 300 m	25.14	13.55	0.413	4.11	43.11	25.75	0.253	4.06	61.31	29.65
H_2 = 500 m	15.63	9.85	0.524	4.80	42.30	22.40	0.302	5.15	48.37	25.70
H_2 = 1500 m	39.55	14.03	0.511	4.71	32.67	24.17	0.370	4.51	30.36	23.85
H_3 = 500 m	20.25	5.40					0.312	4.94	33.83	24.55
H_3 = 1000 m	38.95	22.30					0.408	4.69	43.07	24.90
L_3 = 6 km	36.03	20.90					0.252	5.51	43.85	24.95
L_3 = 18 km	27.83	14.90					0.371	4.32	44.56	24.95

[a]Growth rate and phase speed for case 4a corresponds to the wave that crosses the canyon. Simulations uses base case configuration varying the parameter indicated.

Jordi et al., 2005a]. This approach does not account for net exchange nor the path of the water involved in the exchange. We present here a procedure for diagnosing the cross-shore displacements of the water using an Eulerian passive tracer.

[38] Our results show that unstable fronts and submarine canyons each enhance transports across the shelf break. The volume of water transported across the shelf break represents about the 20% of the volume of water transported alongshelf by the front. However, the offshore exchange induced by the frontal instability is reduced to about 10% of the volume of water transported alongshelf by the front. Furthermore, the canyon does not seem to play an important role in the exchange induced by the unstable front over the canyon. Another difference between the exchange caused by the unstable wave (case 3) and the canyon (case 2) is that frontal instability over the shelf produces an exchange of water over the entire shelf with a relatively small timescale (6 days). The cross-shelf transport induced by canyons is localized in their vicinity and is produced over a relatively large timescale in the absence of other forcing.

4.4. Sensitivity Analysis

[39] We report results of several sensitivity analysis concerning the representation of viscous processes, initial front and shelf and canyon topography in the model for the different base cases described previously. Table 3 presents a selection of these results quantified by the volume of water transported across the shelf break and exchanged between shelf and slope, and growth rate and phase speed of unstable waves.

[40] Viscous processes, whether internal to the fluid or via bottom friction, affect both transports and growth of unstable waves. Transports, exchanges, growth rate and phase speed are basically unaffected by a smaller horizontal eddy viscosity (ν), although they are much weaker for a larger eddy viscosity. An increase of bottom friction (C_d) results in a decrease in transports, exchanges, growth rate and phase speed by extracting energy from the system.

[41] The dependence of the base cases on the magnitude of the frontal parameters is investigated. Increasing the vertical shear of the initial front by increasing the front depth (H_0) results in a dramatic increase in transports, exchanges, growth rate and phase speed. The vertical extent of the influence of the canyon topography is limited by the vertical shear [*Ardhuin et al.*, 1999] and, consequently, increasing vertical shear should decrease the influence of the canyon. In our case, increasing H_0 the vertical shear is significantly increased in the upper layer but it is reduced in the deeper shelf layer and the influence of the canyon is increased. Moreover, increasing vertical shear increases the source of energy for the unstable front being primarily baroclinic. On the other hand, increasing horizontal shear by increasing front width (L_0) results in opposite effects due to the canyon (it increases transports and exchanges) and the frontal instability (it decreases transports and exchanges). The interaction of unstable waves with the canyon follows the effect caused by unstable waves over the shelf indicating that exchanges are mainly produced by unstable waves.

[42] The effect of different shelf topographies is investigated by varying the shelf depth (H_1) and the open ocean depth (H_2). The canyon topography is smaller for a deeper shelf or for a shallow open ocean and, consequently, water transports and exchanges are reduced. The growth rate for the baroclinic instability is greater in both shallow cases due to two effects. One is the reduction in shelf water depth, which leads to a decrease in transports and exchanges. The other is the topographic β effect due to shallow open ocean resulting in a larger transport and exchange of water.

[43] Finally, the sensitivity of canyon topography is studied in relation to stable and unstable fronts over the canyon. A deeper canyon (H_3) enhances transports, exchanges, growth rate and phase speed in both cases. However, the effect of varying the canyon width (L_3) results in a decrease in transports and an increase in exchanges for the stable front and vice versa for the unstable front, indicating that the flow modifications over the canyon

depends on the relation between the canyon geometry and the velocity of the incident flow [*Allen et al.*, 2003]. The effect of different wavelengths for the unstable wave over the canyon (not shown) is similar to that over the shelf topography (Figure 12c), confirming that canyon topography has a minimal effect on exchanges due to instability in absence of other forcing.

5. Conclusion

[44] We have analyzed the interaction of flow produced by an unstable density front with a submarine canyon using a fine-resolution three-dimensional primitive equation coastal ocean model. Model results show the importance of frontal instabilities and submarine canyons in disrupting the geostrophic balance of the frontal flow over the shelf regions. Both, frontal instability and submarine canyons modify the spatial pattern of vertical motions and enhance the exchanges between the shelf and the slope. The combined effect of the unstable waves driven by baroclinic instability and the canyon topography leads to an exchange similar to that produced by the unstable waves. Nevertheless the canyon accelerates the development of wave crests and slows the growth of wave troughs. The solutions exhibit features consistent with other models and observations, which suggest that the coastal ocean model can be used in a front-canyon interaction study.

[45] A relevant topic of this study is the computation of shelf-slope exchanges. We have used two methodologies: the traditional approach of computing transports across the shelf break and, a new approach which accounts for the origin and path of the exchanged water. The application of both methodologies shows that not all of the water transported across the shelf break is effectively exchanged between the shelf and the open ocean. However, as a result of unstable fronts and submarine canyons, coastal water may be rapidly released to the open ocean contributing to the renewal of shelf water. The importance of this result points to a need for accurate observations and numerical simulation of flow in frontal regions with submarine canyons in order to determine their relation to biogeochemical fluxes and climate variability.

[46] **Acknowledgments.** This work has been partially supported by ESEOO (VEM2003–20577–C14–08) project funded by CYCIT and EUR-OCEANS (NoE 511106) projects funded by European Commission (D. G. Research). A. Jordi work was sustained by a Postdoctoral grant from the Spanish Ministry of Science and Education. The authors would like to thank H. J. Xue for supplying the code for the linear stability analysis.

References

Allen, S. E., M. S. Dinniman, J. M. Klinck, D. D. Gorby, A. J. Hewett, and B. M. Hickey (2003), On vertical advection truncation errors in terrain-following numerical models: Comparison to a laboratory model for upwelling over submarine canyons, *J. Geophys. Res.*, *108*(C1), 3003, doi:10.1029/2001JC000978.

Álvarez, A., J. Tintoré, and A. Sabatés (1996), Flow modification of shelf-slope exchange induced by a submarine canyon off the northeast Spanish coast, *J. Geophys. Res.*, *101*, 12,043–12,055.

Ardhuin, F., J. M. Pinot, and J. Tintoré (1999), Numerical study of the circulation in a steep canyon off the Catalan coast, *J. Geophys. Res.*, *104*, 11,115–11,135.

Chen, D., S. G. Horrigan, and D.-P. Wang (1988), The late summer vertical nutrient mixing in Long Island Sound, *J. Mar. Res.*, *46*, 753–770.

Dinniman, M. S., J. M. Klinck, and W. O. Smith Jr. (2003), Cross-shelf exchange in a model of the Ross Sea circulation and biogeochemistry, *Deep Sea Res., Part II*, *50*, 3103–3120.

Gawarkiewicz, G., K. H. Brink, F. Bahr, R. C. Beardsley, M. Caruso, J. F. Lynch, and C.-S. Chiu (2004), A large-amplitude meander of the shelfbreak front during summer south of New England: Observations from the Shelfbreak PRIMER experiment, *J. Geophys. Res.*, *109*, C03006, doi:10.1029/2002JC001468.

Hickey, B. M. (1995), Coastal submarine canyons, paper presented at "Aha Huliko" A Workshop on Flow Topography Interactions, Office of Naval Research, Honolulu, 17–20 Jan.

Hickey, B. M. (1997), The response of a steep-sided, narrow canyon to a time-variable wind forcing, *J. Phys. Oceanogr.*, *27*, 697–729.

Huthnance, J. M. (1995), Circulation, exchange and water masses at the ocean margin: The role of physical processes at the shelf edge, *Prog. Oceanogr.*, *35*, 353–431.

Inman, D. L., C. E. Nordstrom, and R. Flick (1976), Currents in submarine canyons: An air-sea-land interaction, *Ann. Rev. Fluid Mech.*, *8*, 275–310.

Jordi, A., A. Orfila, G. Basterretxea, and J. Tintoré (2005a), Shelf-slope exchanges by frontal variability in a steep submarine canyon, *Prog. Oceanogr.*, *66*, 120–141.

Jordi, A., A. Orfila, G. Basterretxea, and J. Tintoré (2005b), Coastal trapped waves in the northwestern Mediterranean, *Cont. Shelf Res.*, *25*, 185–196.

Klinck, J. M. (1996), Circulation near submarine canyons: A modeling study, *J. Geophys. Res.*, *101*, 1211–1223.

La Violette, P. E., J. Tintoré, and J. Font (1990), The surface circulation of the Balearic Sea, *J. Geophys. Res.*, *95*, 1559–1568.

Millot, C. (1999), Circulation in the Western Mediterranean Sea, *J. Mar. Syst.*, *20*, 423–442.

Onken, R. (1992), Mesoscale upwelling and density fine structure in the seasonal thermocline - A dynamical model, *J. Phys. Oceanogr.*, *22*, 1257–1273.

Péliz, A., J. Dubert, D. B. Haidvogel, and B. Le Cann (2003), Generation and unstable evolution of a density-driven eastern poleward current: The Iberian poleward current, *J. Geophys. Res.*, *108*(C8), 3268, doi:10.1029/2002JC001443.

Rubio, A., P. A. Arnau, M. Espino, M. M. Flexas, G. Jordà, J. Salat, J. Puigdefàbregas, and A. S. Arcilla (2005), A field study of the behaviour of an anticyclonic eddy on the Catalan continental shelf (NW Mediterranean), *Prog. Oceanogr.*, *66*, 142–156.

She, J., and J. M. Klinck (2000), Flow near submarine canyons driven by constant winds, *J. Geophys. Res.*, *105*, 28,671–28,694.

Skliris, N., J. H. Hecq, and S. Djenidi (2002), Water fluxes at an ocean margin in presence of a submarine canyon, *J. Mar. Syst.*, *32*, 239–251.

Spall, S. A., and K. J. Richards (2000), A numerical model of mesoscale frontal instabilities and plankton dynamics: I. Model formulation and initial experiments, *Deep Sea Res., Part I*, *47*, 1261–1301.

Tintoré, J., D.-P. Wang, and P. E. La Violette (1990), Eddies and thermohaline intrusions on the shelf-slope front off the northeast Spanish coast, *J. Geophys. Res.*, *95*, 1627–1633.

Wang, D.-P. (1982), Development of a three-dimensional limited-area (island) shelf circulation model, *J. Phys. Oceanogr.*, *12*, 605–617.

Wang, D.-P. (1993), Model of frontogenesis: Subduction and upwelling, *J. Mar. Res.*, *51*, 497–513.

Wang, D.-P. (1997), Effects of small-scale wind on coastal upwelling with application to Point Conception, *J. Geophys. Res.*, *102*, 15,555–15,566.

Xue, H. J., and G. Mellor (1993), Instability of the Gulf-Stream front in the South-Atlantic Bight, *J. Phys. Oceanogr.*, *23*(11), 2326–2350.

G. Basterretxea, A. Orfila, and J. Tintoré, IMEDEA (CSIC-UIB), Institut Mediterrani d'Estudis Avançats, Miquel Marquès 21, 07190 Esporles, Illes Balears, Spain.

A. Jordi, Marine Sciences Research Center, State University of New York, Stony Brook, NY 11794, USA. (ajordi@notes.cc.sunysb.edu)

J. M. Klinck, Center for Coastal Physical Oceanography, Old Dominion University, Norfolk, VA 23529, USA.